European Polymer Journal 201 (2023) 112566

Contents lists available at ScienceDirect

European Polymer Journal

journal homepage: www.elsevier.com/locate/europolj

Multi-hierarchical nanoparticles with tunable core by emulsion polymerization processes

Jakes Udabe [a], Neha Tiwari [a], Agustin Picco [b], Cristián Huck-Iriart [c,d], Carlos Escudero [d], Marcelo Calderón [a,e,*]

[a] POLYMAT, Applied Chemistry Department, Faculty of Chemistry, University of the Basque Country UPV/EHU, Donostia - San Sebastián, Spain
[b] INIFTA, Instituto de Investigaciones Fisicoquímicas Teóricas y Aplicadas, UNLP-CONICET, La Plata, Argentina
[c] ITECA, Laboratorio de Cristalografía Aplicada, Universidad Nacional de San Martin, Argentina
[d] ALBA Synchrotron Light Source, Experiments Division, Cerdanyola del Vallès, Spain
[e] IKERBASQUE, Basque Foundation for Science, Bilbao, Spain

ARTICLE INFO

Keywords:
Nanoparticle
Core-shell
Emulsion polymerization
Skin penetration

ABSTRACT

Nanoparticles (NPs) with functional cores are gaining research interest due to their advanced architecture. However, exposed reactive groups on NP surfaces can lead to material side reactions and biomedical tissue damage. NPs with multi-hierarchical morphologies can be synthesized by various methods; however, controlling the size and position of the functional groups using conventional and scalable methods is still a challenge. This study explores emulsion-based polymerization methods for producing multi-hierarchical NPs with varying sizes and compositions. We compared micro-, macro-, and semi-batch emulsion polymerization using 2-hydroxyethyl methacrylate (HEMA) and pentafluorophenyl methacrylate (PFMA) as co-monomers. The components present in PFMA can be substituted and are used for post-synthetic functionalization. The results suggest that the architecture of the synthesized NPs is multi-hierarchical, with the substitutable pentafluorophenyl units surrounded by HEMA monomers. Additionally, we evaluated the NPs' ability to enhance dermal drug penetration using nile red as a hydrophobic drug model. Significant variations in skin permeation enhancement properties were observed among the NPs, underscoring the impact of the synthesis method on nanocarriers' drug delivery performance.

1. Introduction

Polymer nanoparticles (NPs) have gained considerable importance over time; these materials possess distinctive physical and chemical properties due to their high surface area and nanoscale size [1]. In the last decade, great efforts have been made to improve the physical and chemical properties of functional materials in industry, medicine, and academia [2–4]. Reactive particles are characterized by the presence of chemically active groups or moieties. These reactive groups can interact with other molecules, surfaces, or environments to undergo various chemical reactions. The field of reactive particles is a multidisciplinary area of research that finds applications in various scientific and industrial domains. Reactive functional groups located at the surface of polymer NPs are particularly interesting, since they allow to engineer the properties of materials in terms of adhesivity, cell and tissue targeting abilities, etc. [3,5,6]. However, certain chemical functionalities such as amines can lead to toxicity if they are located in the NPs' surface, resulting in undesired side effects in host tissues [7,8]. The development of NPs with chemically functionalized cores promotes reduction of cytotoxicity and undesired side reactions, while increasing their dispersability, biocompatibility and chemical stability [3–5,9]. The strategic placement of these reactive moieties within the core of particles is a fundamental consideration, offering a versatile means to prevent side reactions, bolster stability, enhance biocompatibility, and achieve controlled release, tailored to specific application requirements [10]. In summary, the field of reactive particles plays a pivotal role in diverse scientific and industrial contexts such as catalysis, drug delivery, biotechnology, and surface modification.

To date, a wide range of techniques have been used to prepare multi-hierarchical structures, including self-assembly, spray drying,

* Corresponding author at: POLYMAT, Applied Chemistry Department, Faculty of Chemistry, University of the Basque Country UPV/EHU, Donostia - San Sebastián, Spain.
E-mail address: marcelo.calderonc@ehu.eus (M. Calderón).

https://doi.org/10.1016/j.eurpolymj.2023.112566
Received 14 July 2023; Received in revised form 29 October 2023; Accepted 1 November 2023
Available online 5 November 2023

polymerization, and solvent evaporation [9,11–15]. However, fabricating multi-hierarchical NPs with desired sizes and functional groups using conventional and scalable methods has long been a major challenge [5]. Therefore, a common and robust method for fabricating various functional multi-hierarchical NPs is needed.

Among several polymerization techniques that are nowadays used for the synthesis of NPs, emulsion polymerization has shown to have great potential for the synthesis of NPs with controlled morphology [16–19]. Emulsion polymerization is a free-radical polymerization that has a strong reaction heat release capacity in aqueous phase and the ability to form spherical particles. Emulsion polymerization includes several related processes [18]. In this work, the focus has been on micro-emulsion polymerization, macro-emulsion polymerization and semi-batch emulsion polymerization. In micro-emulsion polymerization, a large amount of emulsifier is used so that thermodynamically stable particles with diameters in the range of 10–100 nm can be obtained [20,21]. In macro-emulsion polymerization, in the contrary, smaller amounts of surfactant are used compared to micro-emulsion and NPs in the range of 50–500 nm are obtained [11,20–23]. Finally, semi-batch emulsion polymerization is a modification of the emulsion polymerization process in which at least one of the monomers is added continuously or stepwise, resulting in larger NPs [9,24,25]. As suggested by Asua J *et al.*, [17,19,26] the physicochemical properties of the monomers play a crucial role in the particle morphology that is obtained [18,20,27]. Multi-hierarchical morphology is produced when the interaction of oligoradicals diminishes between the first and the second stage of emulsion polymerization [19,27,28]. Since there are still no head-to-head comparisons of these three afore mentioned methods, in this work the multi-hierarchical morphologies and properties of NPs obtained through the different synthetic techniques will be compared.

In the present work, 2-hydroxyethyl methacrylate (HEMA) and pentafluorophenyl methacrylate (PFMA) were used as a hydrophilic and as hydrophobic co-monomers, respectively. As shown by Lawrence J *et al.* [29], the pentafluorophenyl unit of PFMA is a good leaving group that can be substituted to functionalize the NPs with a wide range of small molecules. The focus of this work is to compare three synthetic routes, for the synthesis of NPs with tunable functional groups in the core, with the aim of protecting them from the external environment. Therefore, the present study will contribute to the development of novel NPs with different sizes and compositions and a post-functionalization method to tune the hindered functional groups. A thorough characterization is performed to decipher the nano-architecture that each emulsion polymerization produces, and a proof-of-concept study is presented to test the capacities of the post-functionalized NPs in terms of their ability to enhance skin penetration of hydrophobic drugs.

2. Materials and methods

2.1. Materials

2-hydroxyethyl methacrylate 97 % (HEMA), bovine serum albumin-fluorescein isothiocyanate conjugate ≥ 98 % (BSA-FITC), L-Arginine methyl ester dihydrochloride ≥ 98 % (AT) (L-Arg· HCl), N,N-methylenebis(acrylamide) 99 % (BIS), Nile Red ≥ 97 % (NR) potassium persulfate ≥ 99 % (KPS), sodium dodecyl sulfonate ≥ 99 % (SDS), sodium hydroxide ≥ 98 % (NaOH) and triethylamine 99 % (TEA) were purchased from sigma-aldrich (Spain). Pentafluorophenyl methacrylate 95 % (PFMA) from TCI (Japan). Deuterated dimethyl sulfoxide ≥ 99 % (DMSO-d_9) from Across organics (Spain). Ethyl acetate HPLC grade, N, N-dimetilformamida Anhydrous, ≥99 % (DMF), sodium chloride ≥ 99 % (NaCl) and tetrahydrofuran Anhydrous, ≥99 % (THF) from Scharlau (Spain). Vivaspin centrifugal concentrator with molecular weight cut-of (MWCO) of 300 kDa and Minisart® SRP25 Syringe 0.45 μm hydrophobic PTFE from Sartorius (Germany). Pig ear skin was obtained from a local slaughter-house.

2.2. Synthesis and post-functionalization of NPs

2.2.1. Synthesis of polymer NPs

The polymer NPs were synthesized using three types of emulsion polymerizations: micro-emulsion, macro-emulsion and semi-batch emulsion polymerization, as shown in Scheme 1.

2.2.2. Synthesis of polymer NPs by micro-emulsion polymerization

Poly(HEMA/PFMA) NPs were synthesized by a batch process in an oil-in-water (O/W) micro-emulsion system containing 10 wt% monomer content, stabilized by ~25 wt% (with respect to total mass) of SDS (More detailed information regarding the quantities can be found in the supporting information (SI) **Table S1**). Potassium persulfate was used as an initiator at a concentration of 2 wt% with respect to the monomer. The experiment was carried out in a 50-mL three-necked round-bottomed flask, equipped with a magnetic stirrer, reflux condenser, thermometer, and gas inlet. Different amounts of HEMA and PFMA were added depending on the formulation in addition to BIS as crosslinker (2 wt%, respect to the monomers). All reactants were dissolved in water and purged with nitrogen for at least 30 min. The solution was placed in a 70 °C oil bath and the polymerization was initiated with KPS and carried out for 6 h under a nitrogen stream and constant stirring at 250 rpm. Finally, the dispersion was purified by dialysis against deionized water for 1 week using Spectra-Por membrane with MWCO of 10 kDa. The reaction yield and the solution concentration were measured by freeze-drying and gravimetric characterization.

2.2.3. Synthesis of polymer NPs by macro-emulsion polymerization

The experimental procedure of macro-emulsion polymerization was similar to the micro-emulsion polymerization. In this procedure, monomer concentration was 70 wt% and the stabilizer concentration (SDS) was ~5 wt% (with respect to total mass) (**SI Table S1**).

2.2.4. Synthesis of polymer NPs by semi-batch emulsion polymerization

Poly(HEMA/PFMA) NPs were synthesized by a semi-continuous process in an oil-in-water (O/W) emulsion system containing 70 wt% monomer concentration and stabilized by SDS (~5 wt%, with respect to total mass) (**SI Table S1**). Potassium persulfate was used as initiator at a concentration of 2 wt% of the total monomer weight. The experiment was carried out in a 50-mL three-necked round-bottomed flask, equipped with a mechanical stirrer, reflux condenser, thermometer, and gas inlet. Initially, different amounts of the monomer PFMA used as the core component was dissolved depending on the formulation. The crosslinker BIS (2 wt%, respect to the monomers) and the surfactant SDS were added to this solution and the temperature was kept at 70 °C and purged with nitrogen for at least 30 min. Initially, 80 % of the initiator was added to the flask. After 20 min, HEMA was added dropwise to the reactor within 60 min (8.3 μL/min) and the remaining initiator (20 %) was added. The system was kept at 70 °C for an additional 2 h to allow it to conduct polymerization. Finally, the dispersion was purified by dialysis against deionized water for 1 week using Spectra-Por membrane with MWCO of 10 kDa. The reaction yield and the solution concentration was measured by freeze-drying and gravimetric characterization.

2.2.5. Post-functionalization of the NPs

L-Arginine methyl ester dihydrochloride (L-Arg · 2HCl) was used to substitute pentafluorophenyl groups to generate positive charges in the NPs. For substitution reaction, similar protocol proposed by other studies was used [30–34]. For this, a stoichiometric amount of L-Arg · 2HCl (3. eq with respect to pentafluorophenyl groups) was taken and neutralized using triethylamine (TEA) before adding to the dispersed NP solution in DMF. The reaction was kept under stirring for 48 h at room temperature. Finally, a 1 M NaOH solution was added to hydrolyze any remaining replaceable group. The final product was obtained with dialysis against deionized water using Spectra-Por membrane with MWCO of 10 kDa for over three days followed by lyophilization.

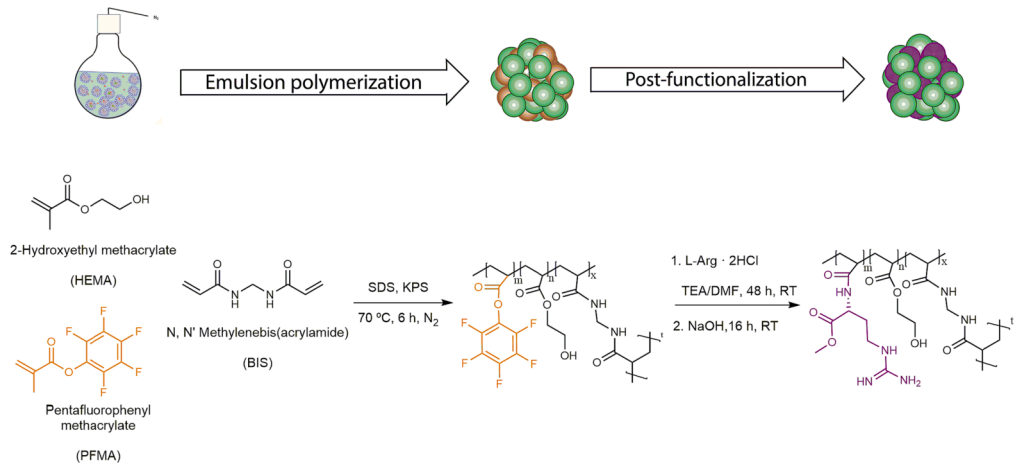

Scheme 1. Proposed reaction for polymeric NP, synthesized by micro-emulsion polymerization, macro-emulsion polymerization and semi-batch emulsion polymerization, and its post-functionalization. Post-functionalization can occur in both amine groups of l-Arg, but it is proposed for clarity, as supported by previous research [30].

2.3. Characterization

2.3.1. Molecular composition and reaction yield

The molecular structure of the NPs was determined using fourier transform infrared spectroscopy (FTIR) (Nicolet™ iS20 FTIR Spectrometer), with a proton-1 nuclear magnetic resonance (^{1}H NMR) (Bruker AVANCE 300), and fluorine-19 nuclear magnetic resonance spectroscopy (^{19}F NMR) (Bruker AVANCE 500). In the case of FTIR, freeze-dried NPs were analyzed. Both ^{1}H NMR and ^{19}F NMR were characterized by dispersing 20 mg of freeze-dried material in 600 μL of DMSO-d_6. The reaction yields were measured by gravimetric after purification and lyophilization process (**Table S2**).

2.3.2. Composition of monomers in polymerized latexes

The composition of the monomers in the polymeric NPs was determined by the FTIR technique [35,36]. For this, calibration curves were generated for each polymeric route, using proportional weight percentage mixtures of pHEMA and pPFMA synthesized by each individual polymeric pathway. Since all formulations contain the same amount of BIS with a band at 1700 cm^{-1} (Amide I band, stretching), the intensities belonging to HEMA (3350 cm^{-1}; alcohol group, stretching) and PFMA (1506 cm^{-1}; pentafluorophenyl aromatic ring, stretching) were normalized with this value.

2.3.3. Size and polydispersity determination

Dynamic light scattering (DLS) was used to obtain the average hydrodynamic diameters of the NPs. A total of 2 mL of the NPs dispersion (1 mg/mL) were added to a polystyrene clear sided cuvette in the case of dispersing the NP in Mili-Q water and a quartz clear sided cuvette in case of dispersing the NP in 90:10 THF:H_2O (V/V%). The sample in the cuvette was well mixed and then the size was analyzed by intensity on a malvern nano zetasizer at an angle of 173° and in the position 4.65 mm height of the plastic cuvette at 25 °C.

2.3.4. Hydrolysis of the activated ester

Malvern nano zetasizer was used to determine surface zeta potential of the NPs. A total of 1 mL of the NPs dispersion (1 mg/mL) in 10 mM of NaCl were added to the disposable folded capillary cells. As shown in similar investigations [37], a tendency towards more negative charges can be directly correlated with the hydrolysis of the pentafluorophenyl methacrylate group, due to the formation of methacrylic acid moieties in the polymer backbone because of the hydrolysis of activated ester in presence of water.

2.3.5. Morphology

Transmission electron microscopy (TEM) was used to observe the morphology of the NPs using Tecnai G2 F20 TWIN microscope. The NP suspensions were diluted to 0.025 mg/mL solution with milliQ water, the suspension was added to a TEM grid for TEM analysis. Small Angle X-ray Scattering (SAXS) measurements were performed in the BL11 NCD-SWEET beamline from the ALBA Synchrotron Light source, Barcelona, Spain (project ID 2021024995). Experiments were done using 2 mm external diameter glass capillaries. The incoming beam energy was set at 12.4 keV with two sample to detector distances in order to cover a wide angular range: 6700 and 2177 mm. 2D patterns were recorded in a Pilatus 1 M (Dectris, Switzerland) detector. Isotropic 2D patterns were integrated using pyFAI library,1 in results the Intensity in function of the scattering momentum transfer q was obtained for each experiment where $q = (4\pi/\lambda)\sin(\theta)$ with λ incoming beam wavelength and 2θ the scattering angle. Several frames ranging from 0.2 to 0.5 s were recorded for each sample in order to analyze possible radiation damage. SAXS experiments were employed to analyze de size distribution in function of the synthesis conditions and processing. Moreover, the globular nature of the building blocks and the overall NPs in solution (hierarchical structures), and their high size polydispersity, the registered intensity was attributed to spheroidal NPs where the diameter size distribution function for each condition was obtained by Montecarlo simulations using McSAS software [38].

2.3.6. Characterization of post-functionalized NPs

To demonstrate the substitution of the pentaflurophenyl units, ^{1}H NMR, ^{19}F NMR, FTIR and surface zeta potential were performed. In the case of FTIR, freeze-dried NPs were analyzed. Both ^{1}H NMR and ^{19}F NMR were characterized by dispersing 20 mg of freeze-dried material in 600 μL of DMSO-d_6. Surface zeta potential was measured by dispersing the NP in 10 mM NaCl solution. It is expected to observe a total disappearance in the ^{19}F NMR signal, due to the absence of pentafluorophenyl groups after post-functionalization. In addition, the bands belonging to amines were observed in ^{1}H NMR and FTIR.

2.3.7. Dermal penetration studies

Skin permeation studies were performed using pig ear skin. Nile red (NR) was used as model of lipophilic drugs to test the penetration enhancement properties of the NPs. NR has been reported to be easily subtracted from the skin with organic solvents and to not penetrate the *stratum corneum* by itself [39,40]. For NR encapsulation, 75 μL methanol solution of NR (1.5 mg/mL) was added into a pre-dispersed NP solution (2 mg/mL in 0. 5 mL 10 mM PBS pH 7.4 solution). The mixture was

vortexed and incubated overnight at 37 °C, protected from the light. After that, it was incubated opened cap at 50 °C for 2 h to remove the remaining methanol, and the dispersion was kept in the fridge overnight at 4 °C. Then, the NPs were filtered and washed with water, removing the insoluble free NR, and the encapsulation efficiency and loading capacity was determined by previously defined calibration curve of NR in ethyl acetate solution.

A support with a 0.75 cm^2 was adhered to the skin using glue. In this area, 150 μL solution of NP (2 mg/mL) with NR encapsulated was deposited and incubated in a temperature gradient from 32 °C to 37 °C for the first 30 min and a constant temperature of 37 °C until 2 h have elapsed. After the incubation time, the skin was cleaned with abundant water to eliminate the NPs and NR that did not penetrate the skin and it was immersed in 2 mL of ethyl acetate for three days to extract the penetrated NR. The loading content was assessed through centrifugation at 13552 × *g* for 10 min, and subsequent characterization was carried out using the supernatant. Subsequently, it was sonicated and filtered using by Minisart® SRP25 Syringe 0.45 μm hydrophobic PTFE, the amount was quantified by absorbance using a quartz cuvette.

3. Results and discussion

In this work, different NPs were designed, varying the composition of the monomers and using three different emulsion polymerization techniques. Due to the different nature of the monomers and the synthesis techniques, a large number of NPs were obtained and compared. The aim of the work was to evaluate which emulsion polymerization method is more reliable to develop NPs with a multi-hierarchical structure, where the replaceable functional group is preferentially located towards the core of the NP. To confirm this, the screening of composition, structure and morphology was done. In addition, the replaceable group of the NPs was modified and characterized.

3.1. Composition of monomers in the polymeric NPs

FTIR spectroscopy was used to quantify the composition of the monomers in the NPs [35,36]. As can be noted in Table 1, an almost total incorporation of both monomers is observed in all formulations and for the three types of polymerizations. Considering that the error of the FT-IR to determine the composition is within 5–10 % [41,42], it can be asserted that the NPs obtained through the three polymeric routes are comparable in their composition.

3.2. Size and polydispersity

In this section, the hydrodynamic diameter of the NPs was measured both in an aqueous medium and in a mixture of THF and water, as the final NPs may contain hydrophobic and hydrophilic domains. shows the hydrodynamic diameter in an aqueous medium and in THF/water mixture. In Fig. 1**(A)** a trend can be seen that by increasing the percentage of HEMA in the polymeric formulation in the three synthetic routes, in the aqueous medium the size is increased in the aqueous medium. On the contrary, despite the fact that aggregations and an increase in polydispersity were observed (**Figure S10, SI**), the opposite trend was obtained by dispersing the NPs in an organic solvent mixture. These tendencies were expected, owing to the nature of the different monomers. On the one hand, nanoparticles with high content of HEMA contains greater amount of a hydrophilic hydroxyl (–OH) groups, which imparts water-attracting (hydrophilic) properties to the polymer. In contrary, THF as a non-polar organic solvent does not have the same affinity for hydrophilic groups. On the other hand, NPs synthesized with PFMA are expected to be highly hydrophobic due to the presence of fluorine atoms. Fluorine is one of the most electronegative elements, and the strong electronegativity of fluorine atoms creates a highly non-polar and hydrophobic environment. As a result, materials containing fluorine tend to repel water and exhibit hydrophobic properties. When it comes to swelling behavior in different solvents like THF and water, the hydrophobicity of the NPs synthesized with PFMA would make them more prone to swelling in non-polar solvents like THF compared to water.

In addition to this, it was observed that when the NPs were dispersed in the aqueous medium, the biggest NPs were synthesized by semi-batch emulsion polymerization, followed by the macro-emulsion polymerization and continuing with micro-emulsion polymerization that generate the smaller NPs. The reason lies in the fact that in semi-batch polymerization one of the monomers was added continuously and slowly; thus, prolonging the nucleation and initiation phase and generating less compact networks and larger NPs [43,44]. In the contrary, in micro-emulsion polymerization, a high amount of surfactant was used, decreasing the surface tension and reducing the size of the micelles, and thus reducing the resulting NP particle size. Finally, no trend was observed regarding polydispersity of the particles in solution.

Table 1
Composition of NP prepared by micro-emulsion polymerization, macro-emulsion polymerization and semi-batch emulsion polymerization as determined by FTIR (Figure S7-9 (SI)).

Feed ratio	Micro-emulsion polymerization		Macro-emulsion polymerization		Semi-batch emulsion polymerization	
	HEMA (%)	PFMA (%)	HEMA (%)	PFMA (%)	HEMA (%)	PFMA (%)
100: 0	90.3 ± 0.7	0.2 ± 0.3	94.8 ± 3.0	0.1 ± 0.1	101.6 ± 2.2	0.9 ± 1.1
80: 20	84.3 ± 7.2	22.2 ± 2.1	83.1 ± 1.9	20.2 ± 10.7	74.4 ± 6.5	9.5 ± 1.5
60: 40	60.9 ± 0.8	38.1 ± 7.4	51.7 ± 5.2	55.1 ± 3.9	53.9 ± 7.5	50.4 ± 13.1
40: 60	48.2 ± 10.3	67.8 ± 9.1	38.9 ± 2.3	57.4 ± 9.7	35.6 ± 3.7	56.3 ± 3.5
20: 80	16.4 ± 9.6	84.6 ± 8.3	25.6 ± 4.9	57.6 ± 3.2	16.2 ± 1.4	75.2 ± 3.5
0: 100	1.4 ± 3.6	95.1 ± 6.9	2.3 ± 2.2	99.3 ± 3.3	1.1 ± 1.5	94.1 ± 5.1

3.3. Morphology

The morphology of the NPs was investigated using SAXS and compared by TEM. In this study, it was desired to obtain a morphology that protects the replaceable group of PFMA. For that, NPs were synthesized using monomers with different degrees of hydrophilicity. As can be seen in Fig. 1 **(C)** and in **Figure S12-13 (SI)**, the NPs were spherical in shape and with similar NP size tendency to those observed with the characterization by DLS. TEM images contrast mainly is dependent on the difference in electron density [45]. It was observed that when the concentration of the fluorinated monomer decreases, the TEM contrast is reduced, since fluorinated moieties produce contrast in this type of microscopy (**Figure S12-13**). Comparable results were obtained by different studies wherein NPs based on PFMA were synthesized [10,29,46–49]. Furthermore, it was noticed that contrasts seemingly increased towards the core of NPs **(Figure S12)**. This is clearer for macro-emulsion NP, thus suggesting that PFMA is preferentially located in the regions least exposed to the surface. This observation implies that PFMA is predominantly situated within the regions of the NPs that are least exposed to the surface.

SAXS curves acquired in aqueous solution for all the NPs can be found in **Figure S11 (SI)**. Roughly, SAXS data replicated the trends observed by DLS. Increasing the content of HEMA in the polymeric formulation caused a shift of the main features in the SAXS curves towards lower q-values, indicating larger dimensions of the NPs. This is illustrated in Fig. 2**,** which shows selected SAXS curves of NPs obtained through macro-emulsion polymerization. At both formulation extremes, i.e. 0:100 and 100:0 (HEMA:PFMA) (wt.%), the SAXS patterns were compatible with (polydisperse) spheroidal objects with homogeneous electron density distribution and with smooth surface. The systematic

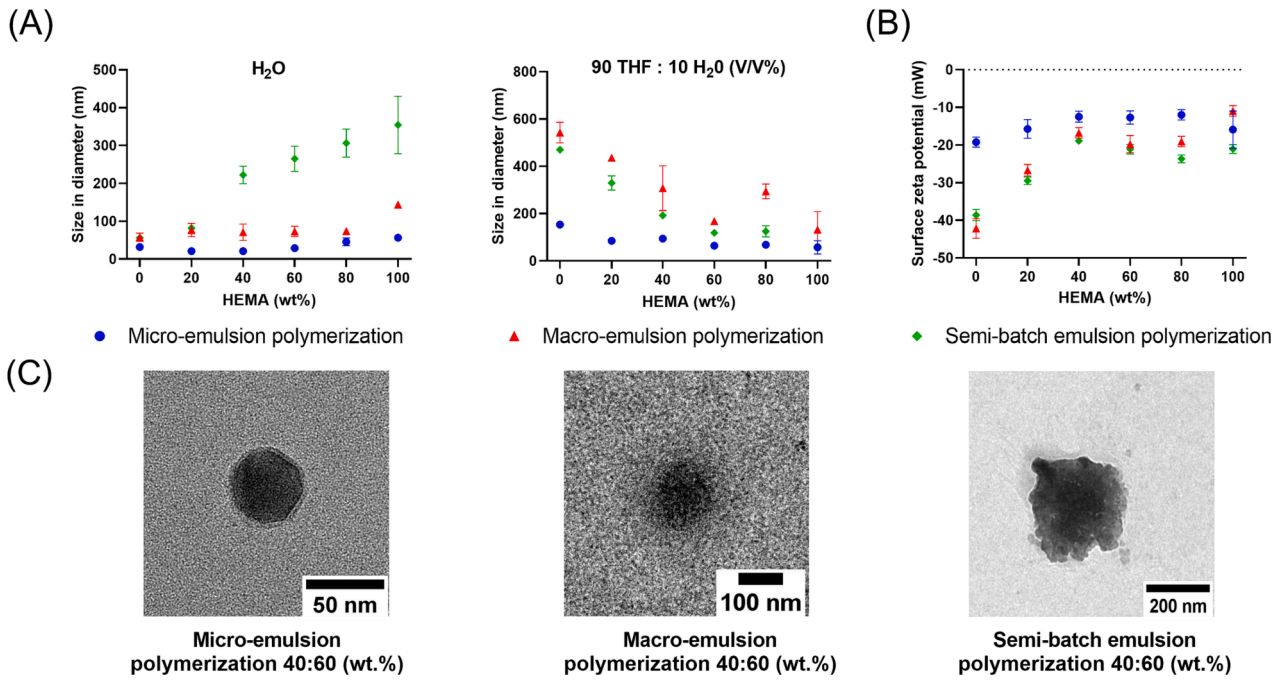

Fig. 1. (A) Diameter in an aqueous medium and in a 90:10 THF: H_20 (V/V%) medium as determined by the intensity distribution in DLS. (B) Surface zeta potential of different NP formulations measured in 10 mM NaCl solution. (C) TEM images of representative NPs synthesized by three routes of emulsion polymerization (More details of other formulation in Figure S12-13 (SI)).

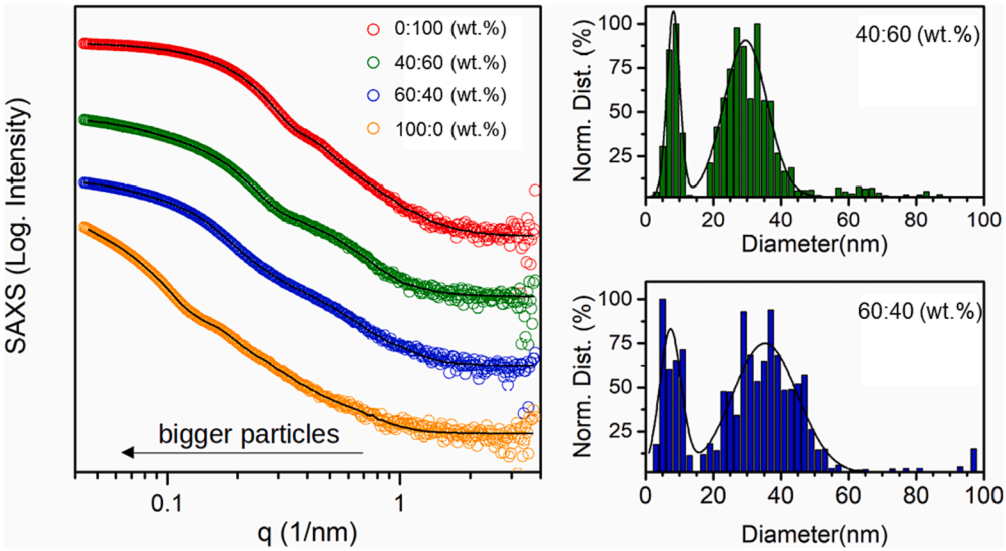

Fig. 2. The left panel shows the SAXS curves of NPs obtained through macro-emulsion polymerization method. The NPs were dispersed in water at 1 g/L for the measurements. Hollow circles represents the experimental data and solid black lines the adjusted curves. The right panels show the obtained volume-based size distribution (bars) for the NPs synthesized by macro-emulsion polymerization having 40:60 to 60:40 (HEMA:PFMA) (wt.%). The distributions were normalized by their maximum. The black lines represents fittings of the obtained distributions using two gaussian contributions. More details of other formulation can be observed in Figure S11 (SI).

shift in the curves to lower angles form 0 % to 100 % HEMA is an indication of the presence of bigger particles. In addition, NPs with intermediate compositions (20:80 to 80:20 (HEMA:PFMA) (wt.%)) presented SAXS curves that were compatible with structures composed of two hierarchical levels [50], the larger one representing the whole particle and the smaller one deriving from internal nanodomain segregation (presumably, PFMA). Considering this, we fit the SAXS curves using the Monte Carlo regression method to retrieve the size distribution of particles with a predetermined geometry implemented in McSAS [51]. Due to the spheroidal nature of the systems, a spherical form factor as scattering contributions was selected. This simple approach was capable of fitting both types of curves (those seen at extreme and intermediate HEMA values) using the same model.

As can be seen, at 0:100 (HEMA:PFMA) (wt.%), monomodal size distributions with mean size between 20 and 50 nm are fitted, when going from microemulsion to conventional emulsion to semi-batch approach were aligned also with the trend observed by DLS for the different synthesis methods. At 100:0 (HEMA:PFMA) (wt.%), size distribution centered at bigger values (>60 nm) are adjusted. In addition, for the NPs having both monomers, in particular at 40:60 to 20:80

(HEMA:PFMA) (wt.%), two populations were observed, the bigger attributed to the whole NP and the smaller to nanodomains within. As an example, Fig. 2 **(right)** presents the size distributions obtained for NPs containing 40:60 to 60:40 (HEMA:PFMA) (wt.%) synthesized through conventional emulsion where two levels are evidenced (the smaller at 7–8 nm and the bigger around 30–35 nm, depending on the case In summary, multilobular NPs with predominantly pentafluorophenyl group oriented towards the inside of the NP were successfully synthesized. However, the hierarchical levels were not clearly seen by TEM. Similar findings were found by other studies with similar nanoparticles [52–54], while various characterization techniques may suggest the presence of specific morphologies, it is noteworthy that in these studies TEM investigations consistently revealed a predominantly homogeneous particle morphology. These findings, consistent with our previous observations, indicate that, when visualized through TEM, the analysis of nanoparticle morphology may present unique challenges in contrast to the conclusions drawn from other characterization methods.

The NPs synthesized by semi-batch emulsion polymerization 80:20 and 100:0 HEMA:PFMA (wt.%) could not be characterized due to their large size or due to the precipitation of larger aggregates. As some studies confirmed [19,27,28], non-equilibrium multilobular morphology are obtained when the interaction of oligoradicals decreases between the first and the second stage of emulsion polymerization. These processes are controlled by the interfacial energy of the system creating multilobular morphologies.

3.4. Stability of the activated ester

As N. Mohr et al. observed in their study [37], pentafluorophenyl moieties are susceptible to hydrolysis forming carboxylic acid moieties in the presence of water, which influence the surface charge. In case of low HEMA content (≥20 wt%) in semi-batch and macro-emulsion polymerization a strong negative potential was observed (Fig. 1 **(B)).** [37]In contrast, other formulations with higher amount of HEMA (wt.%) and micro-emulsion polymerization do not show a tendency towards more negative charges. It is presumed that, micro-emulsion polymerization avoids hydrolysis on the surface of the NP to a greater extent. Probably, the nature of the synthesis suggest that the hydrophobic regions of PFMA have lower exposure in comparison to the other two synthetic pathways. It is worth to mention, that the intrinsic slightly negative charge observed in all NPs may belong to the persulfate groups of the initiator [46].

3.5. Post-synthetic functionalization

As previously discussed, pentafluorophenyl groups are preferentially located in the core of the NPs. Moreover, the corresponding monomers are post-functionalized with a broad variety of commercially available

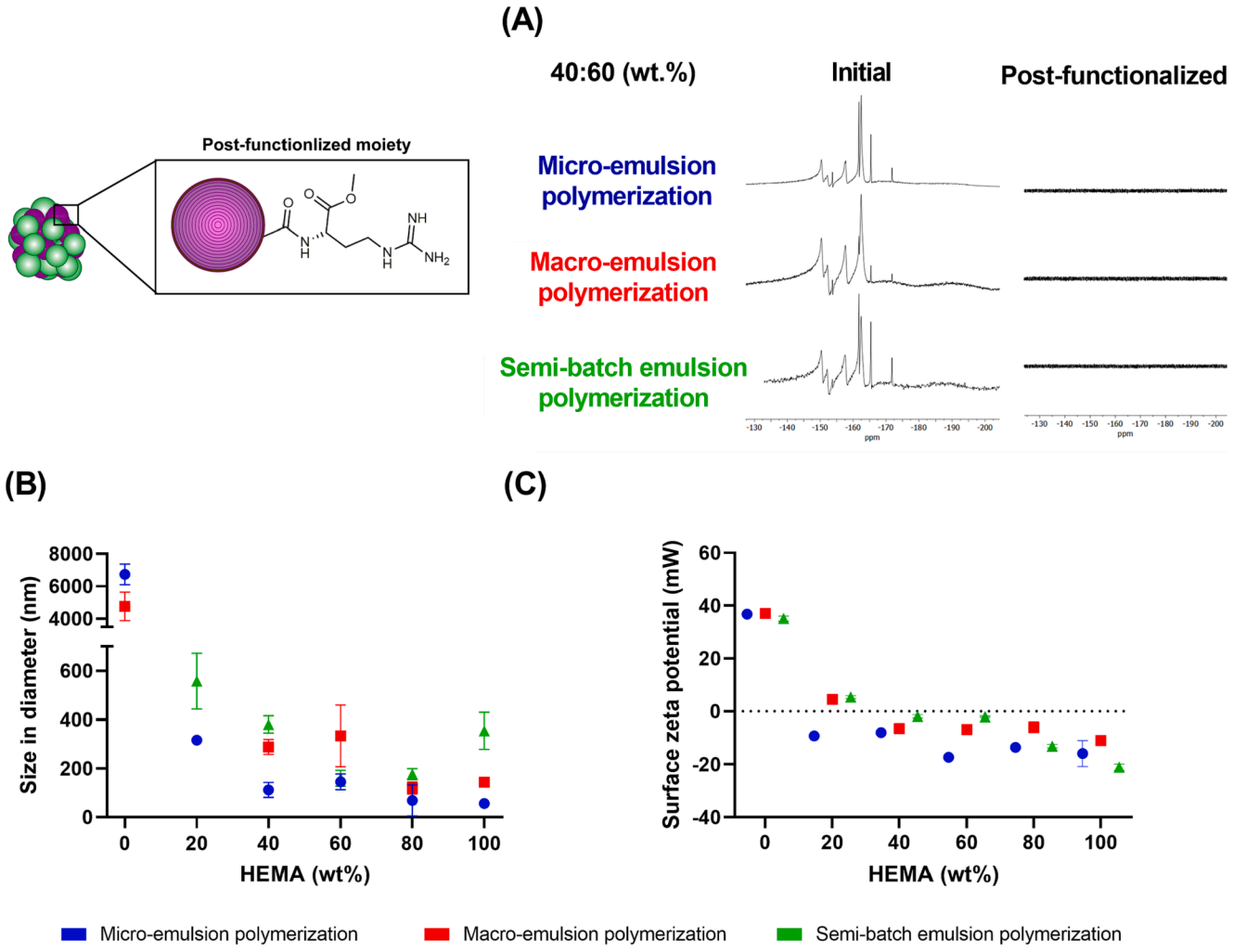

Fig. 3. (A) ^{19}F NMR spectra of 40:60 (wt.%) NPs after and before post-functionalization. (B) Diameter of L-Arg · 2HCl substituted NPs in Mili-Q water measured by intensity. (C) Surface zeta potential of different post-functionalized NPs measured in 10 mM NaCl solution. More details of ^{19}F NMR of other formulation can be found in information (Figures S19-22).

amines and alcohols because the pentafluorophenyl moieties are good leaving groups in nucleophilic substitutions [30]. In this study, L-Arg was used to assay the efficacy of the substitution, as it counts with a nucleophilic center and is a molecule of pharmaceutical interest [52–58]. The chemical composition of the post-functionalized NPs was characterized by FTIR, ^{1}H NMR and ^{19}F NMR. FTIR characterization (**Figures S13-22**), clearly revealed an increase signal at 1700 cm^{-1} (amide I band, stretching) and 3350 cm^{-1} (alcohol group, amino group, stretching) coming from the L-Arg moieties. Moreover, a missing signal from the aromatic ring of PFMA (1506 cm^{-1}; pentafluorophenyl aromatic ring, stretching) was confirmed. In ^{1}H NMR, the existence of amino groups in the system belonging to L-Arg at $\delta = 1.90$ ppm (–NH_2, f, L-Arg) was clearly indicated. In addition to this, the absence of fluorine in the NPs was verified by ^{19}F NMR (Fig. 3**(A)).** Once post-functionalized, the NPs changed their size as observed in the Fig. 3**(B)**. The same tendency was observed by other research groups that post-functionalized pentafluorophenyl containing NPs, probably because this moiety promotes more swelling in the NPs than the pentafluorophenyl moiety [32,33]. Interestingly, the observed trend is that as the HEMA concentration increases, the post-functionalized NPs become smaller. Furthermore, it was observed that only the 100 wt% PFMA NPs drastically changed their surface charge (Fig. 3**(C)**) after post-functionalizing with L-Arg · 2HCl, due to positively charged amino moieties. In addition, it was observed that by decreasing the percentage of PFMA being substituted, the charges on the surface also decrease, being slightly more positive than the initial surface charges. Among the different polymerization techniques used, the same size and surface zeta potential trend was observed after post-functionalization. In summary, since a positive surface charge from the NPs is not observed, it is deduced that the post-functionalized nanodomains are located within the NP.

3.6. Dermal penetration study

To analyze the influence that the hydrodynamic size and the surface chemistry of the NPs may have on their drug delivery capacity, a dermal penetration study of NR encapsulated in the NPs was performed. In several studies, it has been shown that NPs are capable of penetrating the *stratum corneum (SC)* [59–61], for which they have to fulfil the prerequisite to be smaller than $\leq$ 1 μm in diameter [62,63], to have neutral surface charge [64–66], and to be rather lipophilic [67]. Considering this, the synthesized NPs have the potential of improving the permeation of encapsulated drugs, as their size is within the optimal range, and the neutral surface charge is maintained after post-functionalization. In the dermal study carried out according to Fig. 4 **(A),** NPs with a composition 40:60 wt% (HEMA: PFMA) were loaded with NR as model for hydrophobic drugs and were subsequently incubated with pig skin with a temperature ramp 32–37 °C, emulating the natural temperature gradient of the skin. The 40:60 wt% composition was chosen as it better represent the difference in sizes for the differently prepared NPs. As observed in Fig. 4**(B),** in the selected formulation NR was encapsulated with approximately the same amount of LC (%). As shown in Fig. 4**(C)**, it was observed that the NPs synthesized by micro-emulsion polymerization enhance the skin penetration of NR to a greater extent when compared to the other NPs. Micro-emulsion polymerized NPs are the smallest, and as several studies have shown, the NP size is an important parameter to consider for dermal penetration [68,69]. Furthermore, as suggested by some studies [70,71], NPs synthesize by micro-emulsion may have enhanced absorption and penetration in permeable surfaces compared with macro-emulsion NPs. Micro-emulsion systems provide a stable environment for NP formation. Some studies reported that the stability of the NPs synthesized by micro-emulsion could prevent aggregation or coalescence, ensuring that they maintain their small size and high surface area, which is crucial for skin penetration [72–77].

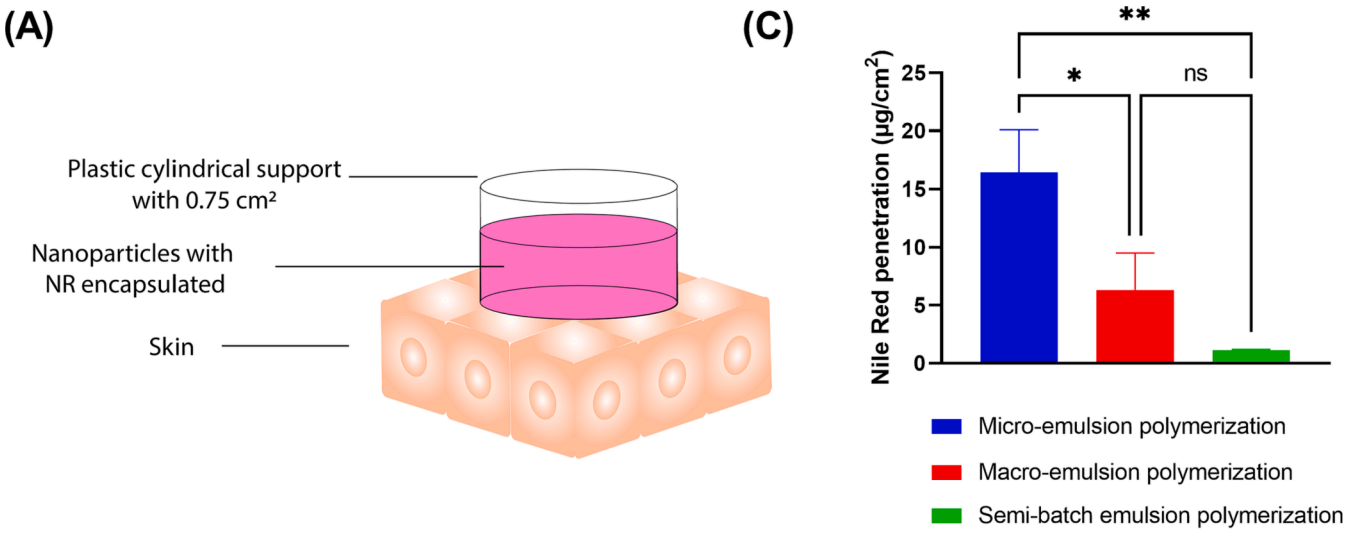

(B)

40:60 wt.%	Encapsulation efficiency (Mean ± SD (%))	Loading capacity (Mean ± SD (%))
Micro-emulsion polymerization	47.94 ± 2.44	2.11 ± 0.10
Macro-emulsion polymerization	44.35± 7.77	1.95 ± 0.33
Semi-batch emulsion polymerization	47.91 ± 6.53	2.10 ± 0.28

Fig. 4. Skin studies of NPs with a composition 40:60 wt% (HEMA: PFMA) (A) NR penetration in pig ear skin, (B) Encapsulation efficiency and loading efficiency of NR in the NPs, (C) NR penetration in the skin.

In addition, Souto E *et al.* [78], described that in similar formulations there is a tendency that as the size of the NP decrease, the penetration is enhanced. In other studies, a similar pattern emerges where a reduction in nanoparticle size corresponds to an increase in skin penetration [62,79–81]. Since NPs synthesized through micro-emulsion polymerization are the smallest, they may enhance penetration greater as compared to the other NPs synthesized with other routes.

Furthermore, it is emphasized that all the employed techniques for synthesizing NPs enable post-functionalization inside the NP. This methodology facilitates the synthesis of NPs specifically tailored for applications in industry, medicine, and research in new material development research [2–4].

4. Conclusions

Novel multilobed NPs composed of tunable moieties were successfully synthesized via three different emulsion polymerization methods. It was suggested that the micro-emulsion polymerization technique avoids hydrolysis on the surface compared to the other routes, thus protecting efficiently the modifiable groups; probably, as already mentioned due to the better homogenization of the system. In addition, it was also observed that the size of NPs could be controlled using different compositions of the monomers. Through TEM and SAXS characterizations, it was suggested that the synthesized NPs were spherical and present a multilobular hierarchy. In addition, in TEM microscopy it was observed that the the replaceable pentafluorophenyl group is predominantly located towards the interior of the NPs. Moreover, the ease of substituting the pentafluorophenyl group with an organic molecule has been demonstrated. It was observed that the surface charge of the post-functionalized changed drastically only in the NP of pPFMA. However, it was corroborated by other techniques the optimal incorporation of L-Arg in all formulations. Thus, demonstrating that the substitution reaction occurred within the core of the NPs. These results indicate that the proposed synthetic methods allows the formation of NPs with modifiable groups and the facility and feasibility of substituting these groups.

Pig ear skin model was used to evaluate dermal penetration studies of potential It demonstrated that NPs synthesized by micro-emulsion polymerization greatly promote the penetration of NR into the skin. As suggested by several studies, micro-emulsion polymerized NPs may enhance significantly the penetration of the cargo because the size and superficial tension of the NPs are lower compared to the other systems.

In conclusion, NPs synthesized by different routes showed to have different physicochemical properties. A difference in size is observed when varying the synthesis where the largest were obtained by semi-batch emulsion polymerization followed by macro-emulsion polymerization and micro-emulsion polymerization, respectively. Furthermore, it has been observed that the synthesis route has an impact on the structure of the nanoparticles, with those synthesized via micro-emulsion polymerization producing NPs where the pentafluorophenyl group is predominantly present in the core.

CRediT authorship contribution statement

Jakes Udabe: Conceptualization, Methodology, Writing – original draft, Investigation. **Neha Tiwari:** Conceptualization, Methodology, Investigation. **Agustin Picco:** Software, Data curation, Methodology, Formal analysis, Writing – review & editing. **Cristián Huck-Iriart:** Software, Data curation, Methodology, Formal analysis, Writing – review & editing. **Carlos Escudero:** Software, Methodology, Formal analysis. **Marcelo Calderón:** Conceptualization, Supervision, Project administration, Funding acquisition, Writing – review & editing.

Declaration of Competing Interest

The authors declare that they have no competing interests.

Data availability

Data will be made available on request.

Acknowledgments

We acknowledge financial support of Basque Health Department (projects 2022333035, 2022333039 and 2022333031), the University of the Basque Country (projects COLLAB22/05 and GIU21/033), IKERBASQUE-Basque Foundation for Science, POLYMAT - Basque Center for Macromolecular Design, MINECO project RTI2018-099227-B-I00 and FPI Fellowship (PRE2019-088584). Small Angle X-ray Scattering (SAXS) measurements were performed in the BL11 NCD-SWEET beamline from the ALBA Synchrotron Light source, Barcelona, Spain (project ID 2021024995) with the collaboration of ALBA staff. The authors thank for technical and human support provided by SGIker (UPV/EHU/ ERDF, EU) for the characterization of transmission electron microscopy measurements. N. Politakos, M.S. Orellano, and B. Espuche are acknowledged for proof reading the manuscript.

Appendix A. Supplementary material

Supplementary data to this article can be found online at https://doi.org/10.1016/j.eurpolymj.2023.112566.

References

[1] I. Khan, K. Saeed, I. Khan, Nanoparticles: properties, applications and toxicities, Arab. J. Chem. 12 (7) (2019) 908–931, https://doi.org/10.1016/j.arabjc.2017.05.011.
[2] D. Geißler, N. Nirmalananthan-Budau, L. Scholtz, I. Tavernaro, U. Resch-Genger, Analyzing the surface of functional nanomaterials—how to quantify the total and derivatizable number of functional groups and ligands, Microchim. Acta 188 (10) (2021) 321, https://doi.org/10.1007/s00604-021-04960-5.
[3] K.S. Kumar, V.B. Kumar, P. Paik, Recent advancement in functional core-shell nanoparticles of polymers: synthesis, physical properties, and applications in medical biotechnology, J. Nanopart. 2013 (2013) 1–24, https://doi.org/10.1155/2013/672059.
[4] R. Kumar, K. Mondal, P.K. Panda, A. Kaushik, R. Abolhassani, R. Ahuja, H.-G. Rubahn, Y.K. Mishra, Core-shell nanostructures: perspectives towards drug delivery applications, J. Mater. Chem. B 8 (39) (2020) 8992–9027, https://doi.org/10.1039/D0TB01559H.
[5] F.M. Galogahi, Y. Zhu, H. An, N.T. Nguyen, Core-shell microparticles: generation approaches and applications, J. Sci.: Adv. Mater. Devices 5 (4) (2020) 417–435, https://doi.org/10.1016/j.jsamd.2020.09.001.
[6] W. Huang, C.P. Tsui, C.Y. Tang, L. Gu, Effects of compositional tailoring on drug delivery behaviours of silica xerogel/polymer core-shell composite nanoparticles, Sci. Rep. 8 (1) (2018) 1–13, https://doi.org/10.1038/s41598-018-31070-9.
[7] E. Fröhlich, The role of surface charge in cellular uptake and cytotoxicity of medical nanoparticles, Int. J. Nanomed. 7 (2012) 5577–5591, https://doi.org/10.2147/IJN.S36111.
[8] F.-F. An, W. Cao, X.-J. Liang, F.-F. An, W. Cao, J.-X. Liang, Nanostructural systems developed with positive charge generation to drug delivery, Adv. Healthc. Mater. 3 (8) (2014) 1162–1181, https://doi.org/10.1002/ADHM.201300600.
[9] W. Huang, Z. Mao, Z. Xu, B. Xiang, J. Zhang, Synthesis and characterization of size-tunable core-shell structural polyacrylate-graft-poly(acrylonitrile-ran-styrene) (ASA) by pre-emulsion semi-continuous polymerization, Eur. Polym. J. 120 (2019), 109247, https://doi.org/10.1016/j.eurpolymj.2019.109247.
[10] A. Gruber, D. Işik, B.B. Fontanezi, C. Böttcher, M. Schäfer-Korting, D. Klinger, A versatile synthetic platform for amphiphilic nanogels with tunable hydrophobicity, Polym. Chem. 9 (47) (2018) 5572–5584, https://doi.org/10.1039/C8PY01123K.
[11] X. Liu, X.-D. Fan, M.-F. Tang, Y. Nie, Synthesis and characterization of core-shell acrylate based latex and study of its reactive blends, Int. J. Mol. Sci. 9 (2008) 9.
[12] M. Fu, J. Huang, S. Feng, T. Zhang, P.C. Qian, W.Y. Wong, One-step solid-state pyrolysis of bio-wastes to synthesize multi-hierarchical porous carbon for ultra-long life supercapacitors, Mater. Chem. Front. 5 (5) (2021) 2320–2327, https://doi.org/10.1039/D0QM00960A.
[13] X. Liu, C. Zheng, X. Luo, X. Wang, H. Jiang, Recent advances of collagen-based biomaterials: multi-hierarchical structure, modification and biomedical applications, Mater. Sci. Eng. C 99 (2019) 1509–1522, https://doi.org/10.1016/J.MSEC.2019.02.070.
[14] L. Wang, W. Wang, W. Cao, H. Xu, Multi-hierarchical responsive polymers: stepwise oxidation of a selenium- and tellurium-containing block copolymer with sensitivity to both chemical and electrochemical stimuli, Polym. Chem. 8 (31) (2017) 4520–4527, https://doi.org/10.1039/C7PY00971B.
[15] X. Cai, J. Dong, J. Liu, H. Zheng, C. Kaweeteerawat, F. Wang, Z. Ji, R. Li, Multi-hierarchical profiling the structure-activity relationships of engineered

nanomaterials at nano-bio interfaces, Nature Communications 9 (1) (2018) 1–12, https://doi.org/10.1038/s41467-018-06869-9.
[16] M. Aguirre, N. Ballard, E. Gonzalez, S. Hamzehlou, H. Sardon, M. Calderon, M. Paulis, R. Tomovska, D. Dupin, R.H. Bean, T.E. Long, J.R. Leiza, J.M. Asua, Polymer colloids: current challenges, emerging applications, and new developments, Macromolecules (2023), https://doi.org/10.1021/ACS.MACROMOL.3C00108.
[17] J.M. Asua, Mapping the morphology of polymer-inorganic nanocomposites synthesized by miniemulsion polymerization, Macromol. Chem. Phys. 215 (5) (2014) 458–464, https://doi.org/10.1002/macp.201300696.
[18] J.M. Asua, Emulsion polymerization: from fundamental mechanisms to process developments, J. Polym. Sci. A Polym. Chem. 42 (2004) 1025–1041.
[19] L.J. Gonzzilez-Ortizt, J.M. Asua, Development of particle morphology in emulsion polymerization. 1. Cluster dynamics, Macromolecules 28 (9) (1995) 3135–3145.
[20] K.C. Ashara, J.S. Paun, M.M. Soniwala, J.R. Chavda, V.P. Mendapara, N.M. Mori, Microemulgel: An overwhelming approach to improve therapeutic action of drug moiety, Saudi Pharmaceut. J. 24 (4) (2016) 452–457, https://doi.org/10.1016/j.jsps.2014.08.002.
[21] A. Gupta, H.B. Eral, T.A. Hatton, P.S. Doyle, Nanoemulsions: formation, properties and applications, Soft Matter 12 (11) (2016) 2826–2841, https://doi.org/10.1039/C5SM02958A.
[22] C. Liu, A.K. Tripathi, W. Gao, J.G. Tsavalas, Crosslinking in semi-batch seeded emulsion polymerization: effect of linear and non-linear monomer feeding rate profiles on gel formation, Polymers (basel) 13 (4) (2021) 1–17, https://doi.org/10.3390/polym13040596.
[23] M. Mirzataheria, A.H. Mahtabanib, M. Lotfalieic, M. Mirzataherid, Emulsion polymerization and encapsulation of micro and nanoparticles within polymer droplets, Jordan J. Chem. 9 (4) (2014) 229–266.
[24] J.W. Vanderhoff, Semi-continuous emulsion polymerization, in: Future Directions in Polymer Colloids, Springer, Netherlands, Dordrecht, 1987, pp. 23–45, https://doi.org/10.1007/978-94-009-3685-0_2.
[25] C.D. Immanuel, M.A. Pinto, J.R. Richards, J.P. Congalidis, Population balance model versus lumped model for emulsion polymerisation: semi-batch and continuous operation, Chem. Eng. Res. Des. 86 (7) (2008) 692–702, https://doi.org/10.1016/j.cherd.2008.01.011.
[26] P.A. Lovell, F.J. Schork, Fundamentals of emulsion polymerization, Biomacromolecules 21 (11) (2020) 4396–4441, https://doi.org/10.1021/acs.biomac.0c00769.
[27] D. Blenner, J. Stubbs, D. Sundberg, Multi-lobed composite polymer nanoparticles prepared by conventional emulsion polymerization, Polymer (guildf) 114 (2017) 54–63, https://doi.org/10.1016/j.polymer.2017.02.080.
[28] A.S. Sonzogni, S. Hamzehlou, V.D.G. Gonzalez, J.R. Leiza, R.J. Minari, Multilobular morphology: the key for biphase multifunctional nanogels, Soft Matter 17 (41) (2021) 9353–9362, https://doi.org/10.1039/D1SM00968K.
[29] J. Lawrence, T. Emrick, Pentafluorophenyl ester-functionalized nanoparticles as a versatile platform for selective and covalent inter-nanoparticle coupling, ACS Appl. Mater. Interfaces 8 (3) (2016) 2393–2398, https://doi.org/10.1021/acsami.5b11550.
[30] M.I. Gibson, E. Fröhlich, H.-A. Klok, Postpolymerization modification of poly (pentafluorophenyl methacrylate): synthesis of a diverse water-soluble polymer library, J. Polym. Sci. A Polym. Chem. 47 (17) (2009) 4332–4345, https://doi.org/10.1002/pola.23486.
[31] C. Battistella, Y. Yang, J. Chen, H.-A. Klok, Synthesis and postpolymerization modification of fluorine-end-labeled poly(pentafluorophenyl methacrylate) obtained via RAFT polymerization, ACS Omega 3 (8) (2018) 9710–9721, https://doi.org/10.1021/acsomega.8b01654.
[32] B. Couturaud, P.G. Georgiou, S. Varlas, J.R. Jones, M.C. Arno, J.C. Foster, R. K. O'Reilly, Poly(pentafluorophenyl methacrylate)-based nano-objects developed by photo-PISA as scaffolds for post-polymerization functionalization, Macromol. Rapid Commun. 40 (2) (2019) 1800460, https://doi.org/10.1002/marc.201800460.
[33] K.A. Günay, N. Schüwer, H.-A. Klok, Synthesis and post-polymerization modification of poly(pentafluorophenyl methacrylate) brushes, Polym. Chem. 3 (8) (2012) 2186, https://doi.org/10.1039/c2py20162c.
[34] A. Gruber, L. Navarro, D. Klinger, Dual-reactive nanogels for orthogonal functionalization of hydrophilic shell and amphiphilic network, Soft Matter 18 (14) (2022) 2858–2871, https://doi.org/10.1039/D2SM00116K.
[35] K. Sakugawa, A. Ikeda, A. Takemura, H. Ono, Simplified method for estimation of composition of alginates by FTIR, J. Appl. Polym. Sci. 93 (3) (2004) 1372–1377, https://doi.org/10.1002/app.20589.
[36] K.I. Ekpenyong, R.O. Okonkwo, Determination of acrylonitrile/methylmethacryiate copolymer composition by infrared spectroscopy, J. Chem. Educ. 60 (1983) 429–430.
[37] N. Mohr, M. Barz, R. Forst, R. Zentel, A Deeper insight into the postpolymerization modification of polypenta fluorophenyl methacrylates to poly(N -(2-hydroxypropyl) methacrylamide), Macromol. Rapid Commun. 35 (17) (2014) 1522–1527, https://doi.org/10.1002/marc.201400249.
[38] I. Bressler, B.R. Pauw, A.F. Thünemann, McSAS: software for the retrieval of model parameter distributions from scattering patterns, J. Appl. Cryst. 48 (3) (2015) 962–969, https://doi.org/10.1107/S1600576715007347.
[39] M. Alhibah, M. Kröger, S. Schanzer, L. Busch, J. Lademann, I. Beckers, M. C. Meinke, M.E. Darvin, Penetration depth of propylene glycol, sodium fluorescein and nile red into the skin using non-invasive two-photon excited FLIM, Pharmaceutics (2022) 14 (9), https://doi.org/10.3390/PHARMACEUTICS14091790.
[40] L. Sheihet, P. Chandra, P. Batheja, D. Devore, J. Kohn, B. Michniak, Tyrosine-derived nanospheres for enhanced topical skin penetration, Int. J. Pharm. 350 (1–2) (2008) 312–319, https://doi.org/10.1016/J.IJPHARM.2007.08.022.
[41] M. Tazreiter, P. Christian, R. Schennach, T. Grießer, A.M. Coclite, Simple method for the quantitative analysis of thin copolymer films on substrates by infrared spectroscopy using direct calibration, Anal. Methods 9 (36) (2017) 5266–5273, https://doi.org/10.1039/C7AY01748K.
[42] D.M. MacKie, J.P. Jahnke, M.S. Benyamin, J.J. Sumner, Simple, fast, and accurate methodology for quantitative analysis using Fourier transform infrared spectroscopy, with bio-hybrid fuel cell examples, MethodsX 3 (2016) 128–138, https://doi.org/10.1016/J.MEX.2016.02.002.
[43] P. Sheikholeslami, C.M. Ewaschuk, S.U. Ahmed, B.A. Greenlay, T. Hoare, Semi-batch control over functional group distributions in thermoresponsive microgels, Colloid Polym. Sci. 290 (12) (2012) 1181–1192, https://doi.org/10.1007/S00396-012-2642-X/TABLES/3.
[44] M. Dulle, S. Jaber, S. Rosenfeldt, A. Radulescu, S. Förster, P. Mulvaney, M. Karg, Plasmonic gold–poly(N-isopropylacrylamide) core-shell colloids with homogeneous density profiles: A small angle scattering study, PCCP 17 (2) (2015) 1354–1367, https://doi.org/10.1039/C4CP04816D.
[45] B. Misof, P. Roschger, P. Fratzl, Imaging mineralized tissues in vertebrates, Comprehen. Biomater. 3 (2011) 407–426, https://doi.org/10.1016/B978-0-08-055294-1.00112-4.
[46] M. Al-Sid-Cheikh, S.J. Rowland, R. Kaegi, T.B. Henry, M.A. Cormier, R. C. Thompson, Synthesis of 14C-labelled polystyrene nanoplastics for environmental studies, Communicat. Mater. 1 (1) (2020) 1–8, https://doi.org/10.1038/s43246-020-00097-9.
[47] S.K. Papadopoulou, I. Karapanagiotis, I. Zuburtikudis, C. Panayiotou, Thermodynamic characterization of poly(2,2,3,3,3-pentafluoropropyl methacrylate), J Polym Sci B Polym Phys 48 (16) (2010) 1826–1833, https://doi.org/10.1002/polb.22053.
[48] A.P.P. Kröger, J.W.D. Paats, R.J.E.A. Boonen, N.M. Hamelmann, J.M.J. Paulusse, Pentafluorophenyl-based single-chain polymer nanoparticles as a versatile platform towards protein mimicry, Polym. Chem. 11 (37) (2020) 6056–6065, https://doi.org/10.1039/D0PY00922A.
[49] K. Han, R. Tiwari, T. Heuser, A. Walther, Simple platform method for the synthesis of densely functionalized microgels by modification of active ester latex particles, Macromol. Rapid Commun. 37 (16) (2016) 1323–1330, https://doi.org/10.1002/MARC.201600213.
[50] G. Beaucage, Combined small-angle scattering for characterization of hierarchically structured polymer systems over nano-to-micron meter: Part II theory, Polymer Sci.: A Comprehen. Ref. 1–10 (1–10) (2012) 399–409, https://doi.org/10.1016/B978-0-444-53349-4.00032-7.
[51] I. Bressler, B.R. Pauw, A.F. Thünemann, McSAS: Software for the retrieval of model parameter distributions from scattering patterns, urn:issn:1600–5767 48 (3) (2015) 962–969, https://doi.org/10.1107/S1600576715007347.
[52] G. Wu, F.W. Bazer, T.A. Davis, S.W. Kim, P. Li, J. Marc Rhoads, M. Carey Satterfield, S.B. Smith, T.E. Spencer, Y. Yin, Arginine metabolism and nutrition in growth, health and disease, Amino Acids 37 (1) (2009) 153, https://doi.org/10.1007/S00726-008-0210-Y.
[53] M.Z. Gad, Anti-aging effects of l-arginine, J. Adv. Res. 1 (3) (2010) 169–177, https://doi.org/10.1016/J.JARE.2010.05.001.
[54] G. Winter, C.D. Todd, M. Trovato, G. Forlani, D. Funck, Physiological implications of arginine metabolism in plants, Front. Plant Sci. 6 (JULY) (2015), 150117, https://doi.org/10.3389/FPLS.2015.00534/BIBTEX.
[55] S.M. Morris, Recent advances in arginine metabolism: roles and regulation of the arginases, Br. J. Pharmacol. 157 (6) (2009) 922, https://doi.org/10.1111/J.1476-5381.2009.00278.X.
[56] R. Geiger, J.C. Rieckmann, T. Wolf, C. Basso, Y. Feng, T. Fuhrer, M. Kogadeeva, P. Picotti, F. Meissner, M. Mann, N. Zamboni, F. Sallusto, A. Lanzavecchia, L-arginine modulates T cell metabolism and enhances survival and anti-tumor activity, Cell 167 (3) (2016) 829–842.e13, https://doi.org/10.1016/J.CELL.2016.09.031.
[57] S.S.A. Mamsa, B.P. Meloni, Arginine and arginine-rich peptides as modulators of protein aggregation and cytotoxicity associated with Alzheimer's disease, Front. Mol. Neurosci. (2021) 14, https://doi.org/10.3389/FNMOL.2021.759729.
[58] M. Tachikawa, S. Hirose, S.ichi Akanuma, R. Matsuyama, K.ichi Hosoya, Developmental changes of L-arginine transport at the blood-brain barrier in rats, Microvasc. Res. 117 (2018) 16–21, https://doi.org/10.1016/J.MVR.2017.12.003.
[59] H.I. Labouta, L.K. El-Khordagui, T. Kraus, M. Schneider, Mechanism and determinants of nanoparticle penetration through human skin, Nanoscale 3 (12) (2011) 4989, https://doi.org/10.1039/c1nr11109d.
[60] R. Banerjee, Overcoming the stratum Corneum barrier: A nano approach, Drug Deliv. Transl. Res. 3 (3) (2013) 205–208, https://doi.org/10.1007/s13346-013-0149-8.
[61] S. Supe, P. Takudage, Methods for evaluating penetration of drug into the skin: A review, Skin Res. Technol. 27 (3) (2021) 299–308, https://doi.org/10.1111/SRT.12968.
[62] M. Schneider, F. Stracke, S. Hansen, U.F. Schaefer, Nanoparticles and their interactions with the dermal barrier, Dermatoendocrinol 1 (4) (2009) 197–206, https://doi.org/10.4161/derm.1.4.9501.
[63] S.S. Tinkle, J.M. Antonini, B.A. Rich, J.R. Roberts, R. Salmen, K. DePree, E. J. Adkins, Skin as a route of exposure and sensitization in chronic beryllium disease, Environ. Health Perspect. 111 (9) (2003) 1202–1208, https://doi.org/10.1289/ehp.5999.

[64] F. Larese Filon, M. Mauro, G. Adami, M. Bovenzi, M. Crosera, Nanoparticles skin absorption: new aspects for a safety profile evaluation, Regul. Toxicol. Pharm. 72 (2) (2015) 310–322, https://doi.org/10.1016/j.yrtph.2015.05.005.
[65] J.P. Ryman-Rasmussen, J.E. Riviere, N.A. Monteiro-Riviere, Penetration of intact skin by quantum dots with diverse physicochemical properties, Toxicol. Sci. 91 (1) (2006) 159–165, https://doi.org/10.1093/toxsci/kfj122.
[66] L.J. Mortensen, S. Jatana, R. Gelein, A. de Benedetto, K.L. de Mesy Bentley, L. A. Beck, A. Elder, L.A. DeLouise, Quantification of quantum dot murine skin penetration with UVR barrier impairment, Nanotoxicology 7 (8) (2013) 1386–1398, https://doi.org/10.3109/17435390.2012.741726.
[67] S.E. Cross, B.M. Magnusson, G. Winckle, Y. Anissimov, M.S. Roberts, Determination of the effect of lipophilicity on the in vitro permeability and tissue reservoir characteristics of topically applied solutes in human skin layers, J. Invest. Dermatol. 120 (5) (2003) 759–764, https://doi.org/10.1046/J.1523-1747.2003.12131.X.
[68] Z. Mardhiah Adib, S. Ghanbarzadeh, M. Kouhsoltani, A. Yari Khosroshahi, H. Hamishehkar, The effect of particle size on the deposition of solid lipid nanoparticles in different skin layers: A histological study, Adv Pharm Bull 6 (1) (2016) 31–36, https://doi.org/10.15171/apb.2016.006.
[69] O. Uchechi, J.D.N. Ogbonna, A.A. Attama, Nanoparticles for dermal and transdermal drug delivery, Applicat. Nanotechnol. Drug Deliv. (2014), https://doi.org/10.5772/58672.
[70] S. Talegaonkar, A. Azeem, F. Ahmad, R. Khar, S. Pathan, Z. Khan, Microemulsions: A novel approach to enhanced drug delivery, Recent Pat. Drug Deliv. Formul. 2 (3) (2008) 238–257, https://doi.org/10.2174/187221108786241679.
[71] Y. Ke, L. Huang, Y. Song, Z. Liu, L. Liang, L. Wang, T. Wang, Preparation and pharmacological effects of minor ginsenoside nanoparticles: A review, Front. Pharmacol. 13 (2022) 2991, https://doi.org/10.3389/FPHAR.2022.974274/BIBTEX.
[72] P. Mohite, T. Rajput, R. Pandhare, A. Sangale, S. Singh, B.G. Prajapati, S. John, S.S. K. Patel, Nanoemulsion in management of colorectal cancer: challenges and future prospects, Nanomanufacturing 3 (2) (2023) 139–166, https://doi.org/10.3390/NANOMANUFACTURING3020010.
[73] B. Nikolaev, L. Yakovleva, V. Fedorov, H. Li, H. Gao, M. Shevtsov, Nano- and microemulsions in biomedicine: from theory to practice, Pharmaceutics (2023) 15 (7), https://doi.org/10.3390/PHARMACEUTICS15071989.
[74] N. Tiwari, E.R. Osorio-Blanco, A. Sonzogni, D. Esporrín-Ubieto, H. Wang, M. Calderón, Nanocarriers for skin applications: where do we stand? Angew. Chem. Int. Ed. 61 (3) (2022) e202107960.
[75] M.S.Z. Shiri, W. Henderson, M.R. Mucalo, A review of the lesser-studied microemulsion-based synthesis methodologies used for preparing nanoparticle systems of the noble metals, Os, Re, Ir and Rh, Materials 12 (12) (2019) 1896, https://doi.org/10.3390/MA12121896.
[76] T. Qin, L. Goual, M. Piri, Z. Hu, D. Wen, Nanoparticle-stabilized microemulsions for enhanced oil recovery from heterogeneous rocks, Fuel 274 (2020), 117830, https://doi.org/10.1016/J.FUEL.2020.117830.
[77] E.B. Souto, A. Cano, C. Martins-Gomes, T.E. Coutinho, A. Zielińska, A.M. Silva, Microemulsions and nanoemulsions in skin drug delivery, Bioengineering 9 (4) (2022), https://doi.org/10.3390/BIOENGINEERING9040158.
[78] E.B. Souto, A. Cano, C. Martins-Gomes, T.E. Coutinho, A. Zielińska, A.M. Silva, Microemulsions and nanoemulsions in skin drug delivery, Bioengineering 9 (4) (2022) 158, https://doi.org/10.3390/BIOENGINEERING9040158.
[79] P. Ghasemiyeh, S. Mohammadi-Samani, Potential of nanoparticles as permeation enhancers and targeted delivery options for skin: advantages and disadvantages, Drug Des. Devel. Ther. 14 (2020) 3271–3289, https://doi.org/10.2147/DDDT.S264648.
[80] J. Yokota, S. Kyotani, Influence of Nanoparticle Size on the Skin Penetration, Skin Retention and Anti-Inflammatory Activity of Non-Steroidal Anti-Inflammatory Drugs, J. Chin. Med. Assoc. 81 (6) (2018) 511–519, https://doi.org/10.1016/J.JCMA.2018.01.008.
[81] L. Liu, W. Zhao, Q. Ma, Y. Gao, W. Wang, X. Zhang, Y. Dong, T. Zhang, Y. Liang, S. Han, J. Cao, X. Wang, W. Sun, H. Ma, Y. Sun, Functional nano-systems for transdermal drug delivery and skin therapy, Nanoscale Adv 5 (6) (2023) 1527, https://doi.org/10.1039/D2NA00530A.